Near Surface Geophysics

EAGE EUROPEAN ASSOCIATION OF GEOSCIENTISTS & ENGINEERS

Near Surface Geophysics, 2021, **19**, 603–623 doi: 10.1002/nsg.12172

Archaeogeophysical exploration in Neuss-Norf, Germany using electrical resistivity tomography and magnetic data

Ismael M. Ibraheem*, Rainer Bergers and Bülent Tezkan

Institute of Geophysics and Meteorology, University of Cologne, Cologne, 50969, Germany

Received February 2021, revision accepted July 2021

ABSTRACT

A combination of electrical resistivity tomography (ERT) and magnetic gradiometry was selected to examine a hypothesis concerning the presence of remains of one of the oldest archaeological churches in the Rhineland, located in Neuss-Norf, Germany. The gradiometer survey was carried out to measure the vertical gradient of the magnetic field using a proton precession magnetometer along several profiles. The magnetic data were reduced to the magnetic pole; then analytic signal and power spectrum techniques were applied. The ERT survey was based on the magnetic results, and both Wenner and dipole–dipole configurations were employed to collect the apparent resistivity data along 12 ERT profiles. The field ERT data from these two arrays were merged into one dataset to form a non-conventional mixed array. The robust (blocky) inversion technique was applied to the resistivity data in order to derive the two-dimensional resistivity distribution of the subsurface. Despite the noisy surroundings, the magnetic survey was able to give an indication of potential walls of the ancient church in addition to several subsurface magnetic sources. Moreover, highly resistivity anomalies were observed within the first 1–2 m of the subsurface soil and were interpreted as possible remains of man-made structures. This depth range was also confirmed by the spectral analysis of the magnetic data. A strong consistency between the two methods was observed in some locations of the site. In addition, the ERT measurements confirm and complement most of the magnetic results. We successfully detected anomalous zones that could be associated with the walls of at least one ancient church building in addition to several possible archaeological structures in the survey area.

Key words: Archaeogeophysics, ERT, Magnetic, Mixed array, Norf - Germany.

INTRODUCTION

Over the past few years, non-destructive geophysical exploration methods have been developed and adopted rapidly for examining shallow-buried structures and remains in archaeological sites (Piro, 2009). Archaeological excavation is, fundamentally, a laborious and invasive process and can cause serious and irreparable damage to the buried archaeological remains. Geophysical methods can therefore serve as fast, cheap and nondestructive tools in determining locations for prospective excavation (Reynolds, 2011; Gündoğdu *et al.*, 2017; Karaaslan and Karavul, 2018). A number of geophysical techniques have been used to investigate archaeological sites, including direct current resistivity, magnetic, ground-penetrating radar (GPR), electromagnetic, microgravity and seismic methods (Jeng *et al.*, 2003; Rizzo *et al.*, 2005; Batayneh *et al.*, 2007; Müller *et al.*, 2009; Zhao *et al.*, 2013; Rabbel *et al.*, 2014; Martinez *et al.*, 2015; Di Maio *et al.*, 2016; Gündoğdu *et al.*, 2017; Akca *et al.*, 2019; Florio *et al.*, 2019; Křivánek, 2019; Lulewicz *et al.*, 2019; Orlando *et al.*, 2019; Yilmaz *et al.*, 2019). Ultimately, the adoption of geophysical techniques in archaeology is not only to the advantage of archaeologists, but also constitutes a precious

*Email: ismael.ibraheem@geo.uni-koeln.de

Figure 1 Location map of the study area. The yellow rectangle marks the location of the archaeological site

resource for decision-makers involved in the protection of human heritage (Hegyi *et al.*, 2019).

Buried archaeological features can be detected using geophysical techniques because of their physical properties contrast with the surrounding soil (Drahor, 2019). However, it is important to note that each individual geophysical method has its limitations due to the assorted range of physical heterogeneity in the subsurface of the archaeological site (Piro *et al.*, 2019). A combination of several geophysical techniques can therefore give a powerful approach to overcome this problem, providing significant complimentary information about archaeological structures before the excavation process begins (Cardarelli *et al.*, 2008; Epov et al, 2016; Piro *et al.*, 2019).

In urban areas, unwanted cultural magnetic noise can be reduced by using a vertical magnetic gradiometer configuration without losing the signal of archaeological information (Ciminale and Gallo, 2008). However, the presence of an archaeological site in an urban area represents a great challenge for carrying out proper magnetic measurements. Several visible metallic objects together with moving vehicles constitute strong sources for noise preventing the executing of an appropriate magnetic survey. Therefore, a high degree of awareness of the difficulty of such measurements should be considered during the acquisition, processing and interpretation of magnetic data.

THE NORF ARCHAEOLOGICAL SITE: LOCALITY AND HISTORICAL BACKGROUND

The area investigated (Fig. 1) is a historical estate in the old part of the parish of Norf, an urban district in Neuss, Germany. It occupies an area of 45 × 30 m^2 that rises about 2 m higher than the surrounding terrain. The area is currently a local park with tombstones and trees, but no signs or remains of a church. There are some suggestions that the potential church could be older than Lambertus-Chapel in Ramrath, seven kilometers from Norf, dating from the ninth or tenth century (Boele, 1997), which is currently believed to be the oldest church in the district. Norf's importance stems from its location between the cities of Neuss and Cologne. The region was under the governance of the Roman Empire in the period between the first and fourth centuries, when military bases and settlements were founded in these cities. This was followed by the Frankish period (fifth to ninth century). Many archaeological finds reported in Pütz (1974) confirm activity in Norf in these periods.

According to Fischer (1989), bigger farmsteads were developed during the Frankish period and some of them included small churches. Directly adjacent to the explored site is a farm called Norfer Hof, which – according to archaeological finds – has existed at least since the Frankish period. This

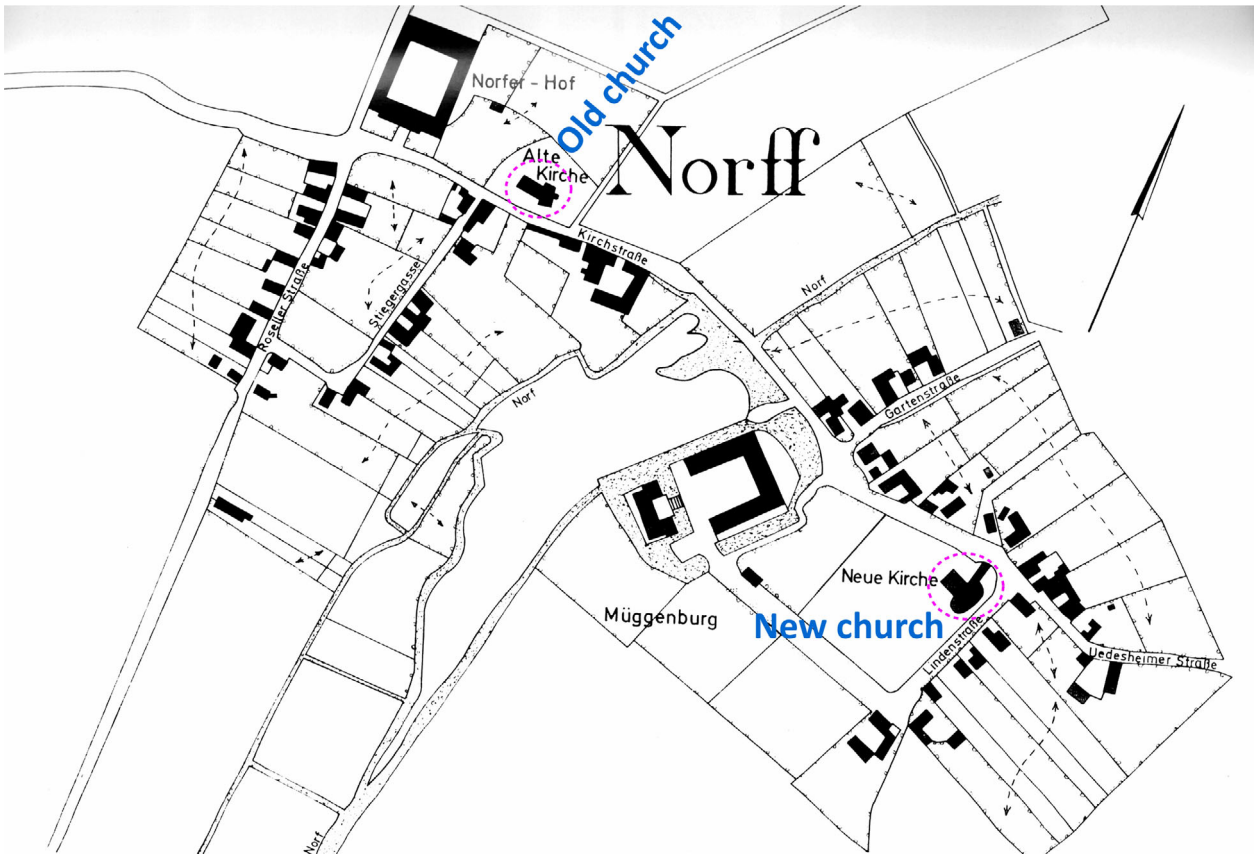

Figure 2 Ground plot of Norf based on the cadastral land register from 1812 showing the locations of the old and new churches (after, Pütz, 1974)

suggests that the potential building, old St. Andreas, possibly originated from that age. The oldest document currently known mentioning the name St. Andreas connected to this district is dated 817 (Lacomblet, 1840). Although this document is somewhat vague, Fischer (1989) combines this with other insights and concludes that it is likely that a church building already existed here in 817. The church has an expected size of 25 m × 7–8 m. The basis for this estimation is a comparison of the St. Andreas church drawn on a map plotted in 1808 with the building still existent on Norfer Hof (Remmen, 2013). A copperplate engraving created in 1586 shows a map, including a schematic figure of the church. According to this, the church was built in an east–west direction, with a massive stump tower in the west (Fischer, 1989; Metzdorf, 2019). During the period from 1765 to 1770, a new, bigger church was built a few hundred meters away from the old church. A map showing the locations of the old and new churches (Fig. 2) was produced in 1812. The old St. Andreas church fell into disuse and was pulled down in 1839 due to its ruinous condition (Pütz, 1974). Here, it is worth mentioning that a road widening process was reported in 1954/1955; therefore, the location and the width of the old road (Kirchstraße) are different from its current ones.

In 1585, the conflict between Catholic and Protestant potentates led to considerable losses in Norf (Pütz, 1974), including the burning of the St. Andreas church (Emsbach and Tauch, 1986). This event potentially influences our research. A document from the year 1586 states that the Archbishop of Cologne gave a directive towards clerics from the superior monastery of Neuss to return to their place. Accordingly, St. Andreas church and other buildings in Norf were reconstructed (Landesarchiv NRW, 2020). Unfortunately, there is no information about the construction process and it is still vague whether the church was reconstructed in the same place or a new church was built close to the original one.

A woman's grave of the Frankish period was found in the 1920s in the neighbouring property. Furthermore, parts of skeletons were reported during roadwork directly adjacent to the investigated site in 1954/1955. These and other

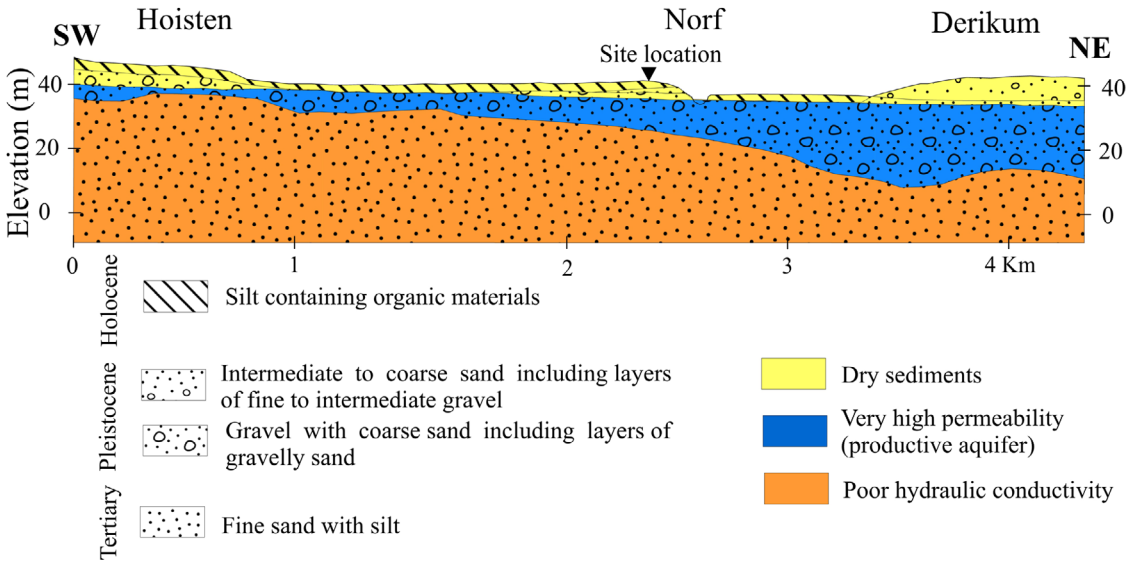

Figure 3 Geological and hydrogeological cross section passing very close to the investigated archaeological site (modified after Geologischer Dienst NRW, 1983)

details about historic findings around the investigated area are described in Siegmund (1998) and Pütz (1974). Unfortunately, no information about the typical size of graves is reported.

According to archaeology experts, the walls of the early churches in the study region were most likely made of wood, later natural stones such as sandstone, tuff, shale, greywacke and so on were used in the construction works, but after the fourteenth century the use of baked bricks became popular in construction. In the case of tombs having masonry walls, they were mostly made from baked bricks, while natural stones were rarely used for this purpose (Weber, 2020).

GEOLOGY OF THE SITE

The geology of the Norf area consists of fluvial terrace sediments, mainly from the Rhine and other smaller streams (Geologischer Dienst NRW, 1983). The Rhine is only 3 km away from the site. An inspection of the geological cross section (Fig. 3) shows that the investigated area is located on a hill to the west of a small stream. The top layer consists of dry sediments, of which the uppermost formation are Holocene fluvial silts containing organic material with a thickness of approximately 1 m (Geologischer Dienst NRW, 1931). The sand below this layer forms the Rhine Pleistocene terraces. The sediments become gradually coarser with depth, that is from silty sand to coarse sand with gravel and, finally, to gravel with coarse sand. This gravelly sand layer represents a productive groundwater aquifer with a thickness of 10–15 m. A Tertiary layer of fine sand with silt forms the base of the aquifer and is characterized by poor hydraulic conductivity. The groundwater level is expected at a depth of approximately 8 m below the ground surface (Geologischer Dienst NRW, 1983). Since the investigated site can be an artificial topographical feature to protect the church from flooding, it is likely that the upper layer is an anthropogenic soil overlying the silt layer.

GEOPHYSICAL METHODS

Non-invasive techniques such as magnetic and electrical resistivity tomography (ERT) geophysical techniques have been widely used in archaeological exploratory studies and have also been employed in the current research as well. A combination of these techniques is believed to give reasonable information about the Norf archaeological site. Examples in the literature about the integration of these methods for archaeological prospecting are reported in articles by Drahor *et al.* (2008), Quesnel *et al.* (2011), Di Maio *et al.* (2016), Fauchard *et al.* (2018), Getaneh *et al.* (2018) and Karaaslan and Karavul (2018) and others.

Magnetometry in archaeological prospecting

Since their introduction, magnetic methods have become the backbone of archaeological prospecting (Piro, 2009). Magnetic surveys are generally employed to determine spatial variations in the earth's magnetic field resulting from local changes

in total magnetization (Schmidt, 2009). By analysing magnetic anomalies, we can eventually reveal the presence of subsurface archaeological remains. To achieve this, a clear magnetic contrast between the archaeological structures and the hosting medium is required (Di Maio *et al.*, 2016). This contrast is generated naturally and anthropogenically. Trenches filled with topsoil, intrusive structures (walls and foundations), fireplaces, pottery and bricks constitute typical examples of anthropic features (Piro, 2009; El-Qady *et al.*, 2019).

Generally speaking, the magnetic intensity of a buried body depends on the magnetization contrast and the depth of the body. Deep sources produce broad anomalies, while shallow sources create narrow and focused anomalies (Telford *et al.*, 1990; Reynolds, 2011). The amplitudes of magnetic anomalies range between a few or tenths of nT (graves and walls) to hundreds of nT (pottery, kilns and other baked objects) and up to few thousands of nT in case of buried ferromagnetic metallic objects (Florio *et al.*, 2019). Negative magnetic anomalies can be obtained over walls of sandstone or limestone (Quesnel *et al.*, 2011; Ayad and Bakkali, 2018).

In magnetometry, the influence of the diurnal variations on the two sensors is identical because of the small distance between them; therefore, measuring the vertical gradient of the magnetic field using two sensors aligned vertically provides a significant advantage because it automatically eliminates both the diurnal variations of the earth's magnetic field and the background magnetic fields (Linsser, 1970; Sharma, 1997; Rizzo *et al.*, 2005; Milsom and Eriksen, 2011; Hinze *et al.*, 2013). It also increases the spatial resolution of the high-frequency shallow anomalies associated with archaeological sources, which are often masked by noise with respect to the low-frequency deep-seated sources of geological origin (Lowrie, 2007; Florio *et al.*, 2019). The difference between the magnetic intensity values recorded by the two sensors, divided by the distance between them gives the vertical magnetic gradient at the mid-point between the sensors (Reynolds, 2011):

$$\partial M/\partial z \approx \Delta M/\Delta \mathrm{z} \; = \; (M_1 - M_2)\,/\Delta \mathrm{z} \qquad (1)$$

where M_1 and M_2 are the total magnetic fields at the lower and upper sensors, respectively; Δz is the distance between the sensors. Details on the theoretical principles regarding magnetometry can be found in the geophysical literature (e.g., Sharma, 1997; Reynolds, 2011; Milsom and Eriksen, 2011).

The current magnetic survey was carried out in order to detect the possible buried church walls in addition to other potentially related archaeological relics. Prior to the survey, we carefully cleaned the area from disturbing magnetic bodies visible on the surface of the ground. The vertical gradient of the magnetic component was measured with a fixed distance of 1.04 m between the sensors. The lower sensor of the gradiometer was set up at a height of 0.32 m from the ground level. The measurements were carried out using the Gem-System GSM-19T Proton magnetometer. The instrument has a sensitivity of less than 0.1 nT, making it suitable to the purpose of archaeological prospecting. A setting for the most accurate readings (4 s cycling time per measured point) was used. During the test measurements, we observed sharp spikes in the magnetic data. These spikes were coming from the passing nearby cars. However, magnetic measurements can be influenced by vehicles at distances of up to 20 m (Milsom and Eriksen, 2011). Though a base station is not necessary in gradiometry measurements, a second magnetometer of the same type was used to record temporal changes in the magnetic field, in order to detect any distortion resulting from active cultural noise (vehicles). The time and the amplitude of these sharp spikes can then be seen on the diurnal variation curve (Fig. 4). Hence, the influence of vehicles on the magnetic measurements was recorded. We avoided measurements during times when cars drove along the road adjacent to the study area. Thus, the measurements were realized during less active cultural noise. However, some spikes produced by far passing vehicles were manually removed from the data.

A local Cartesian coordinate system was set out on the site for the collecting of magnetic and ERT data. Figure 5 shows the layout of the ERT and magnetic surveys. Several plastic measuring tapes formed a grid 38 × 22 m^2. Small wooden sticks were used to permanently fix the sides of the grid for the duration of the survey. The magnetic survey was executed along 27 parallel profiles oriented approximately N80E–S80W with a length ranging from 20 to 37.5 m. The difference in the length of the profiles was due to natural and man-made obstacles. Some parts of the site could not be covered by the measurements due to the presence of trees. According to historical information (see, Fig. 2), the southern part of the area is the expected location of the church. More attention was therefore paid to this area. A spacing of 0.5 and 1.0 m between adjacent profiles was chosen for the southern and northern parts, respectively. A spatial sampling interval of 0.5 m along each profile was selected, which would be adequate for determining large structures such as ancient buildings and tombs.

Like in other geophysical methods, pre-processing of the magnetic data is a prerequisite before the actual processing phase. Through this, all effects not associated with buried archaeological structures should be removed. The magnetic

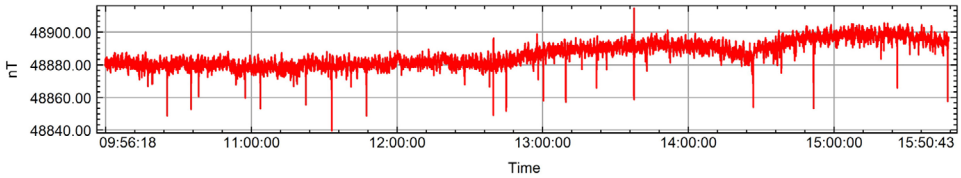

Figure 4 Diurnal variations of the earth's magnetic field at the base station. The effects of passing vehicles on the adjacent road (approximately 24 m from the sensor) on our magnetic measurements appear as sharp spikes on the diurnal variation curve

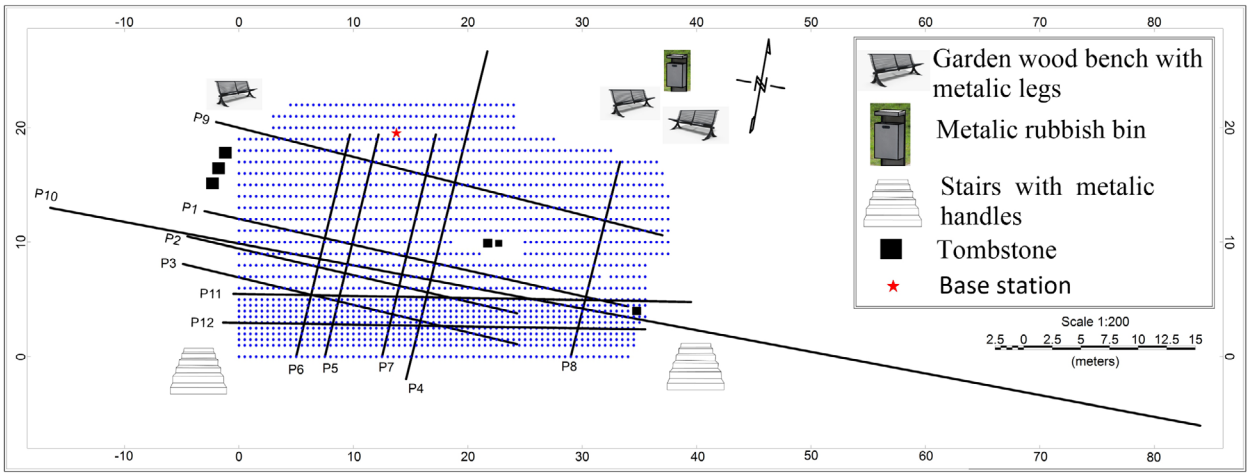

Figure 5 Scheme showing the local coordinate system for collecting magnetic and ERT data. Black lines represent the ERT profiles while blue dots represent the magnetic stations

data were inspected manually, and data associated with noise sources were removed. Then a non-linear spatial de-spiking filter was applied to automatically replace the iron spikes usually existing in gradiometry data with the mean of the adjacent values. The resultant data were gridded using the minimum curvature method and then mapped as shown in Figure 6(a). The minimum and maximum recorded values of the vertical gradient magnetic field are −700 nT/m and 751 nT/m, respectively. The most important features on this map are two clearly distinguishable magnetic zones divided by a negative linear structure trending in the E–W direction. Several dipolar and isolated highly positive magnetic anomalies, presumably associated with buried metallic bodies, and other magnetic features can be recognized on the magnetic map. To overcome the distortion caused by the inclination of the earth's magnetic field and to re-position magnetic anomalies directly over their sources, the magnetic data were transferred to the frequency domain using fast Fourier transform (FFT), then a reduction to the north magnetic pole (RTP) filter was applied assuming that the sources have no remanent magnetization (Baranov and Naudy, 1964; Rajagopalan, 2003; Ibraheem *et al.*, 2018a; Ibraheem *et al.*, 2019a, 2019b). RTP filtering is a fundamental process, which allows a more precise estimate of the location of magnetic sources than the total magnetic intensity data. It removes the dipolar nature of magnetic anomalies; only true dips (associated with asymmetric anomalies) can be seen on the RTP magnetic map (Isles and Rankin, 2013). Values of 66.46° and 2.03° were used for the inclination and the declination of the magnetic field, respectively. Analysis of the RTP vertical gradient magnetic map (Fig. 6b) clearly shows that the area is characterized by several distinguishable magnetic anomalies with different polarizations, shapes and amplitudes ranging from −545 nT/m to +885 nT/m. This map reflects a northward shift in the locations of the magnetic anomalies and a visually enhanced image compared with the vertical gradient magnetic map (Fig. 6a). Moreover, the RTP magnetic data clearly show that the area is divided into two distinct E–W trending sectors; one in the south (zone 1) and the other to the north (zone 2). However, the southern part exhibits a high density of magnetic anomalies, which could possibly be associated with the location of the potential targets. Three discernible bipolar magnetic anomalies denoted B1, B2 and B3 can be seen on the map, reflecting large magnetic sources dipping towards the east or possessing a remanent magne-

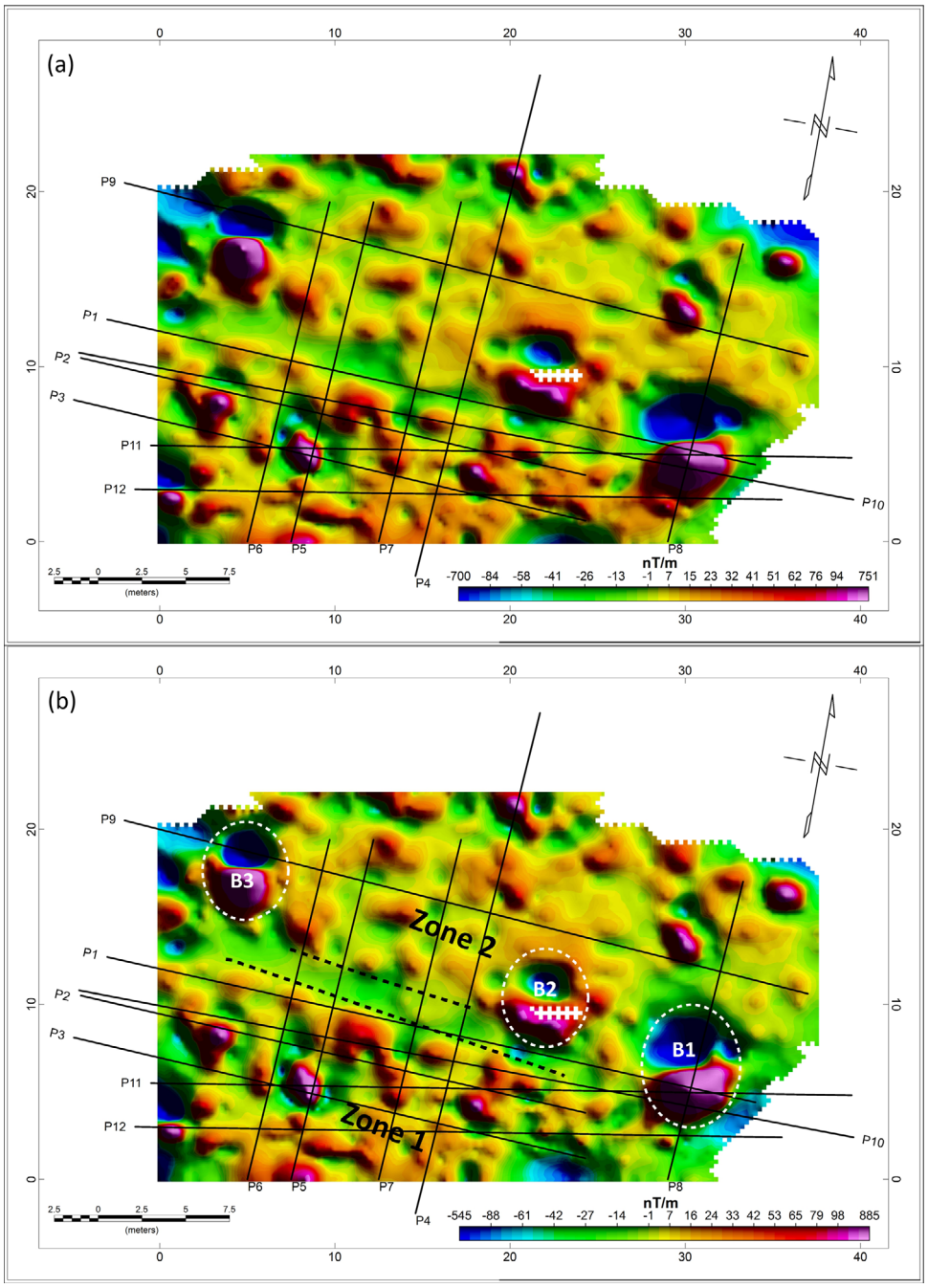

Figure 6 (a) Vertical gradient and (b) RTP vertical gradient magnetic maps of the archaeological site. Lines represent the location of ERT profiles. A negative magnetic belt between two highly magnetic zones can be clearly seen on the map. Dashed black lines show the boundaries of this belt

tization in this direction. It is worth noting that these high magnetic values are not coming from the surface, rather they are generated from metallic materials in the subsurface. However, because the area has been open to the public for centuries, they are possibly but not necessarily of archaeological origin. Also, the archaeological epoch cannot be determined. This represents one of the drawbacks of the current study. The validity of the anomaly B2 is still more questionable and lower than that of B1 and B3 due to the absences of the magnetic data in a small area occupied by trees and gravestones

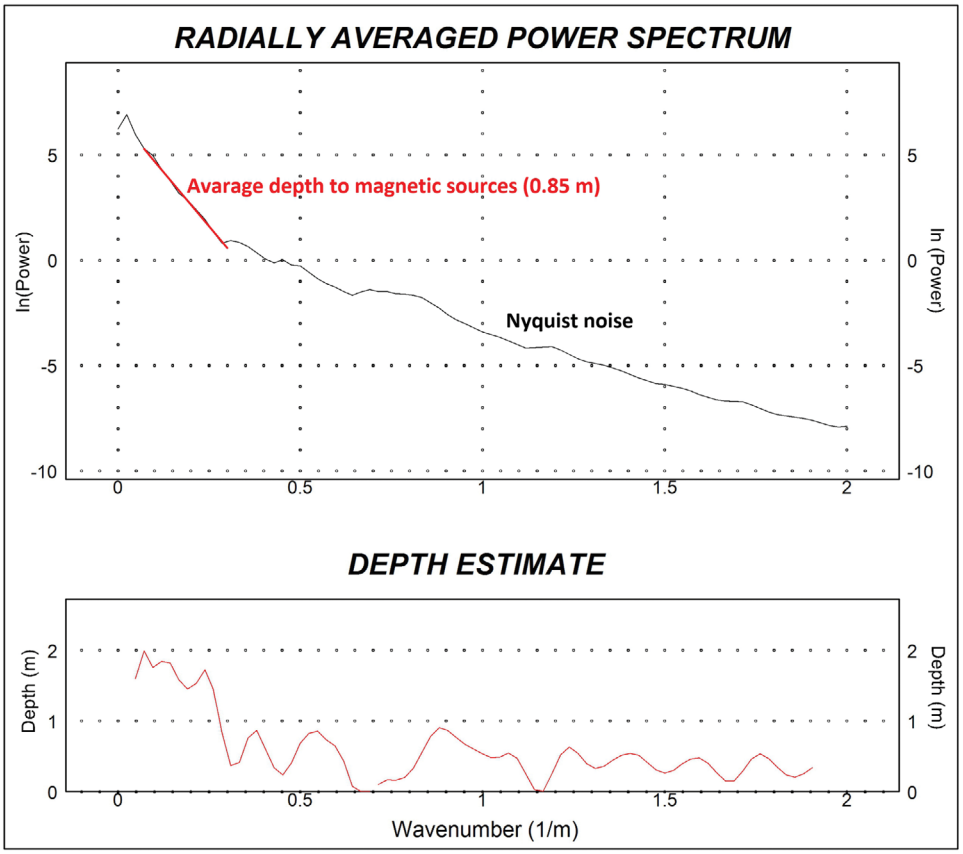

Figure 7 2D radially averaged power spectrum. Average depth to magnetic sources was calculated from the ground surface

preventing the acquisition of data (refer to Fig. 5). Moreover, several moderate to small magnetic anomalies are distributed all over the magnetic map. According to archaeology experts, the typically used materials for walls built after the fourteenth century are baked bricks. The range of magnetic values for such buried archaeological structures is mostly in the range of ±15 nT (Scollar *et al.*, 1990), and in some cases can reach several tens of nT (El Emam *et al.*, 2014). In general, the overprinting of low amplitude anomalies by large ones (possibly produced by metallic sources) in several places in the investigated site makes the interpretation of magnetic data quite difficult and more challenging.

Spectral analysis

The spectral analysis technique was used in order to determine the depth of the buried magnetic sources (Bhattacharyya, 1966; Spector and Grant, 1970; Cassano and Rocca, 1975; Hahn *et al.*, 1976; Fedi *et al.*, 1997; Ghazala *et al.*, 2018; Ibraheem *et al.*, 2018b). The power spectrum of the magnetic data is the product of the two-dimensional (2D) Fourier transform and its complex conjugate. Several depth ensembles can be acquired, based on the slopes (S) of the segments of the power spectrum (Kivior and Boyd, 1998). The depths to magnetic sources are calculated using the following formula (Hinze *et al.*, 2013; Ibraheem *et al.*, 2018a):

$$Depth\ z = -\frac{S}{4\pi} \tag{2}$$

The 2D radially averaged energy–power spectrum curve of our magnetic data (Fig. 7) was generated after applying the FFT to the RTP magnetic data. The first segment of the curve (deep magnetic sources) did not consider in our calculations, and only wavenumbers between 0.1 and 0.3 m^{-1} were considered in order to avoid over-interpretation based on possible aliasing effects. Calculations show that the average depth to magnetic sources from the ground surface is 0.85 m.

Analytical signal

The amplitude of the analytical signal (also called the total gradient) for three-dimensional (3D) structures is given by

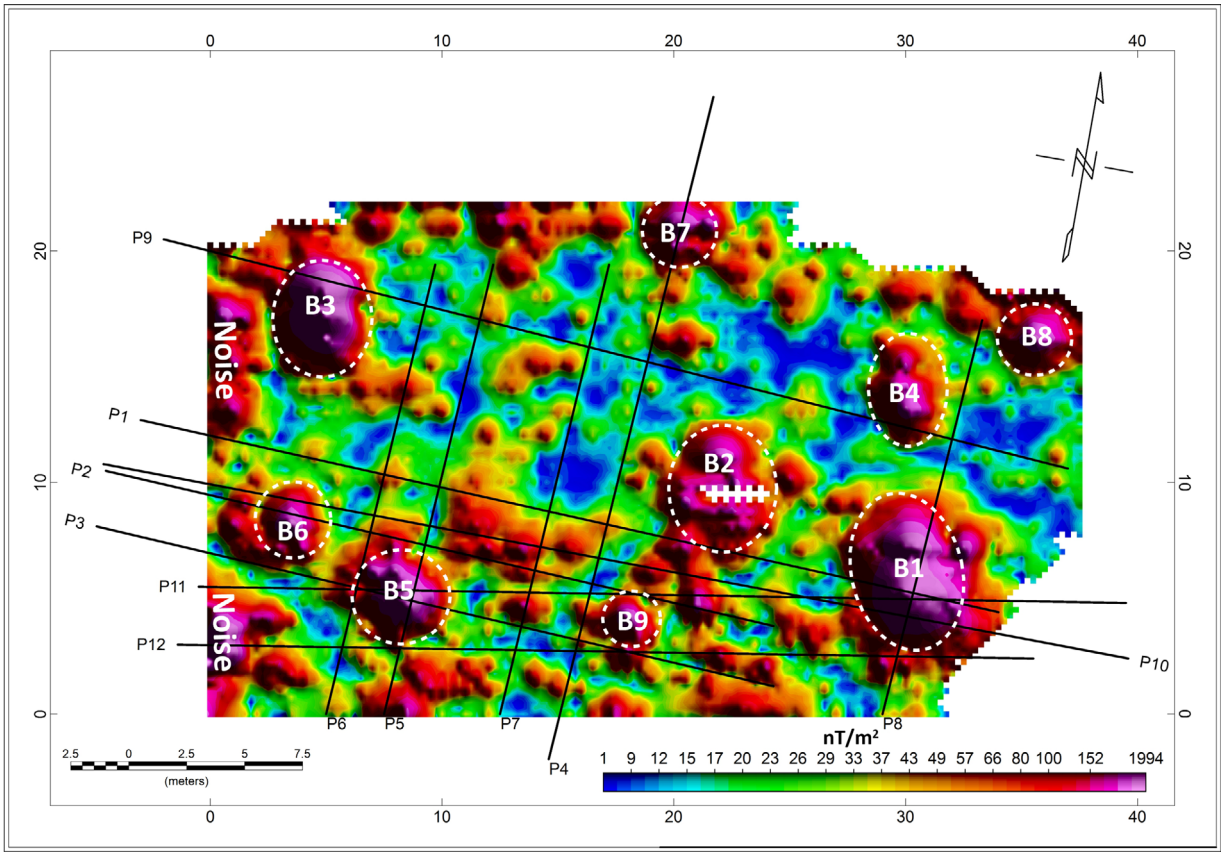

Figure 8 Analytical signal map of magnetic data at Norf archaeological site. Black lines represent the course of the ERT profiles. Dashed white lines refer to interpreted causative magnetic sources. Magnetic anomalies B1–B4 are probably produced by buried metallic bodies and B5–B9 are other strong magnetic anomalies

the following expression (Roest *et al.*, 1992; Ibraheem *et al.*, 2019a):

$$AS(x, y) = \sqrt{\left(\frac{\partial M}{\partial x}\right)^2 + \left(\frac{\partial M}{\partial y}\right)^2 + \left(\frac{\partial M}{\partial z}\right)^2}, \quad (3)$$

where AS(x,y) is the amplitude of the analytic signal, M is the measured magnetic field at (x, y), and $\partial M/\partial x$, $\partial M/\partial y$ *and* $\partial M/\partial z$ are the two horizontal and vertical derivatives of the measured field, respectively.

The amplitude of the AS filter peaks and produces bell-shaped anomalies over magnetic sources. Therefore, its maxima are very powerful in determining the edges of magnetic bodies (Nabighian, 1972), especially for those of shallow depths (Jeng *et al.*, 2003; Arisoy and Dikmen, 2013) irrespective of the orientation of the body's magnetization (Isles and Rankin, 2013). It is clear that the AS map of the Norf archaeological site (Fig. 8) shows the presence of several highly magnetic anomalies (B1–B9), which could indicate shallow buried magnetic sources of different sizes and depths in the study area. Most of these anomalies can be seen on the RTP magnetic map (Fig. 6b). The most interesting are the three anomalies (B1–B3), which distribute on the E–W trending line passing through the centre of the map. These anomalies are clearly seen on the RTP magnetic map as dipolar magnetic anomalies and can possibly be explicated as magnetic sources of metallic nature. High-amplitude anomalies at the western parts of the AS magnetic map are interpreted as noise because they are very close to the metallic handles of the stairs and several tombstones (refer to Fig. 5).

According to archaeologists familiar with this part of the Rhineland, caskets are likely to be endowed with handles and other fittings consisting of iron. Also, caskets made of lead and metallic grave goods, such as parts of livery, were not unusual. An example of such ferromagnetic materials is a sword and a spearhead from the seventh century, which were found in a grave 2 km away from the study location (Marzinkowski, 2020). A modelling study was carried out to calculate the vertical gradient magnetic response of such a sword at several

depths. Its dimensions were inferred from a published picture of the previously mentioned archaeological sword. It was modelled as tubular shape oriented in the E–W direction and dipping 20° towards the east with a thickness of 1 cm, length of 0.5 m and width of 3.5 cm. Values of 48946 nT, 66.4° and 1.9° were considered for the intensity, inclination and declination of the magnetic field, respectively. A susceptibility value of 250 SI (Billings *et al*., 2006; Sanchez *et al*., 2006) was assigned to the modelled object. As a result, the obtained vertical gradient magnetic values generated by the body at depth of 0.5 m (1.34 m from the midpoint between the sensors) range from −16 nT/m to +129 nT/m. These values are much lower than the amplitude values of anomalies B1, B2 and B3, which indicates that swords cannot produce such high anomalies.

Moreover, engravings of some existing tombstones show dates of the nineteenth and early twentieth centuries; this means a younger overprinting of older features must be taken into account. Furthermore, because the area has been open to the public for centuries, other buried metallic objects are thinkable, which in archaeological interpretation is considered being noise.

Two-dimensional electrical resistivity survey

ERT methods have been widely used as powerful tools in archaeological prospecting in order to provide high-resolution images of the subsurface (Hawamdeh *et al*., 2015; Sapia *et al*., 2017; Tsokas *et al*., 2018; Yilmaz *et al*., 2019). ERT is an active geophysical technique for imaging subsurface structures by using multi-electrode electrical measurements made at the surface. It relies on the presence of a resistivity contrast between the buried archaeological structures and the hosting medium (Reynolds, 2011). The detection of archaeological structures using resistivity exploration is sometimes difficult because of resistivity variations of subsurface soils associated with local lithology types and water saturation. Therefore, anomalies caused by the archaeological context may easily be concealed under such conditions. Moreover, the type of electrode configuration plays an important role in defining the resistivity values of the archaeological remains and their hosting medium (Drahor *et al*., 2008; Oswin, 2009). The superiority of any electrode configuration is based on its horizontal and vertical resolution, data coverage and investigation depth, which play a main role in defining the proper array. The Wenner array has a good signal/noise ratio and is less sensitive to horizontal changes in the resistivity. Hence, it resolves vertical changes with a good resolution and, therefore, it is a very suitable choice in noisy areas. When good horizontal resolution and data coverage are required, choosing the dipole–dipole configuration will be the right decision (Loke, 1999, 2020). The final decision of choosing the proper configuration has to be made according to the aim of the survey, the geology of the area, and other field considerations. For more details about the advantages and disadvantages of electrode configurations, refer to Zhou and Dahlin (2003), Dahlin and Zhou (2004) and Loke (2020). Generally, in archaeology, the existence of a high apparent resistivity anomaly refers to a resistive construction such as a cavity, a wall, a grave or a foundation hosted within a less resistive medium (Cozzolino *et al*., 2018).

In archaeological sites, lateral and vertical variations of the subsurface formations are generally expected. Hence, the use of a single configuration will not be adequate in order to achieve precise results. To improve the efficiency of our ERT results, a combined dataset in a non-standard general array format (mixed array) with an increased number of data levels was created using a mixture of measurements from the Wenner and dipole–dipole arrays (Loke, 2000). Kaufmann and Quinif (2001) and Zhou *et al*. (2002) have employed this kind of composite/mixed array to detect sinkholes and found that it is more effective than individual arrays. This procedure has the advantage of increasing subsurface data coverage (i.e., increasing the number of data points in the subsurface within unit depth) as well as providing good horizontal and vertical resolution. This results in an enhanced 2D resistivity image of the subsurface that is superior to the image obtained by individual array inversion; sensitivity is increased, and uncertainty is reduced by combining the vertical resolution of the Wenner array and the horizontal resolution of the dipole–dipole array (Zhou *et al*., 2002). This leads to more realistic imaging and interpretation of the revealed anomalies (Ibraheem *et al*., 2021).

Due to the area's elevation, rainwater can flow outwards from the surface very easily. The surficial soil is therefore very dry compared to the surroundings. The presence of trees in the measuring area may constitute an additional reason for dryness. The dryness of the subsoil causes problems in coupling the electrodes during the measurements, so a small amount of fresh water was applied to improve this process. Overall, the measuring area is very flat except for the side close to the road which has a sloping topography. Therefore, topography measurements were carried out to be incorporated in the inversion process.

The current geoelectrical survey was based on the results of the magnetic survey and was carried out along 12 profiles (Fig. 5). The design of the ERT survey took into consideration that the ERT profiles should correspond to the potential

Table 1 Overview of measured profiles with the mixed array in the ERT survey using the Res2DInv software

Profile	Length (m)	Electrode spacing (m)	Absolute error
P1	37.5	0.5	1.8
P2	29.5	0.5	1.9
P3	30	0.5	1.8
P4	29.5	0.5	2
P5	20	0.5	1.3
P6	20	0.5	1.4
P7	20	0.5	1.3
P8	17.5	0.5	1.7
P9	40	0.5	1.6
P10	102	1.5	4.4
P11	40	1	2.4
P12	37	1	1.8

ancient walls as perpendicularly as possible and cut through the most interesting magnetic anomalies in the archaeological location. The standard Wenner and dipole–dipole configurations were applied to all measured profiles using ABEM Terrameter LS. The distance between each electrode was 0.5 m, and the roll-along procedure was used to extend the length of the profiles and gain a good resolution near the surface at their beginnings and ends (ABEM, 2010). In the current research, a non-conventional mixed array was used for all profiles during the processing of the ERT data. The apparent resistivity data obtained from the Wenner and the dipole–dipole arrays were combined in one dataset for further processing. The data were processed with the RES2DINV software (Loke, 2000) using the robust (L1-norm) inversion technique (Wolke and Schwetlick, 1988) in order to create a reasonable 2D geoelectric model for the distribution of the true resistivity along each profile. Since a considerable resistivity contrast between anthropogenic structures and hosting medium is expected, the robust (blocky) inversion was chosen because it tends to produce models with sharper edges and generally better imaging results than the smoothness-constrained least-squares (L2-norm) inversion (Loke *et al.*, 2003; Dahlin and Zhou, 2004). This makes it more suitable for archaeological investigations (Berge and Drahor, 2011). The accuracy of the data fit is expressed in terms of the absolute error, which provides a scale of the absolute differences between the measured and calculated resistivity data and an indication about the quality of the model obtained (Claerbout and Muir, 1973).

By inspection of the apparent resistivity pseudo-sections, bad datum points were removed manually. Moreover, data values with a highly normalized standard deviation (variation coefficient) in addition to negative apparent resistivity values were also deleted from the dataset. An overview regarding the length, electrode spacing, number of iteration, and absolute error for each ERT profile can be seen in Table 1. The absolute error values obtained for the 2D ERT inverted sections range between 1.3% and 2.4% overall ERT traverse lines. One exception is Profile P10 with an absolute error of 4.4%, which could be due to the surficial lateral resistivity variations along this long profile.

All of the ERT profiles show near-surface features, probably corresponding to man-made structures in addition to a very resistive layer (reaching several thousands of Ωm in some profiles) with a depth of 2–4 m. It was not clear whether this resistive layer is a natural geological layer or an archaeological construction. Therefore, Profile P10 of Figure 5 was constructed as a long reference profile with a length of 102 m and an electrode spacing of 1.5 m to investigate subsurface formations (Fig. 9). Although the subsurface geological structure is the same, some discrepancies between the inverted resistivity models from the Wenner and dipole–dipole arrays are observed (see Fig. 9). The most remarkable discrepancies are highly resistive structures of the shallow subsurface between distance 73 m and distance 85 m along profile P10. Moreover, the overall 2D resistivity image in the mixed model is consistent with the available geological information (see, Fig. 3). The mixed array was therefore chosen to perform the inversion process for all profiles. An inspection of profile P10 shows that the resistivity depth section beneath the investigated site consists of four layers, from top to bottom: (i) A relatively intermediate resistivity layer (average resistivity of 300 Ωm) with a thickness of 0.5–2.5 m. This layer contains local low and high electrical anomalies and can be interpreted as anthropogenic soil. (ii) A relatively low resistivity layer (<100 Ωm down to 10 Ωm). It can be interpreted as a silt layer. (iii) A

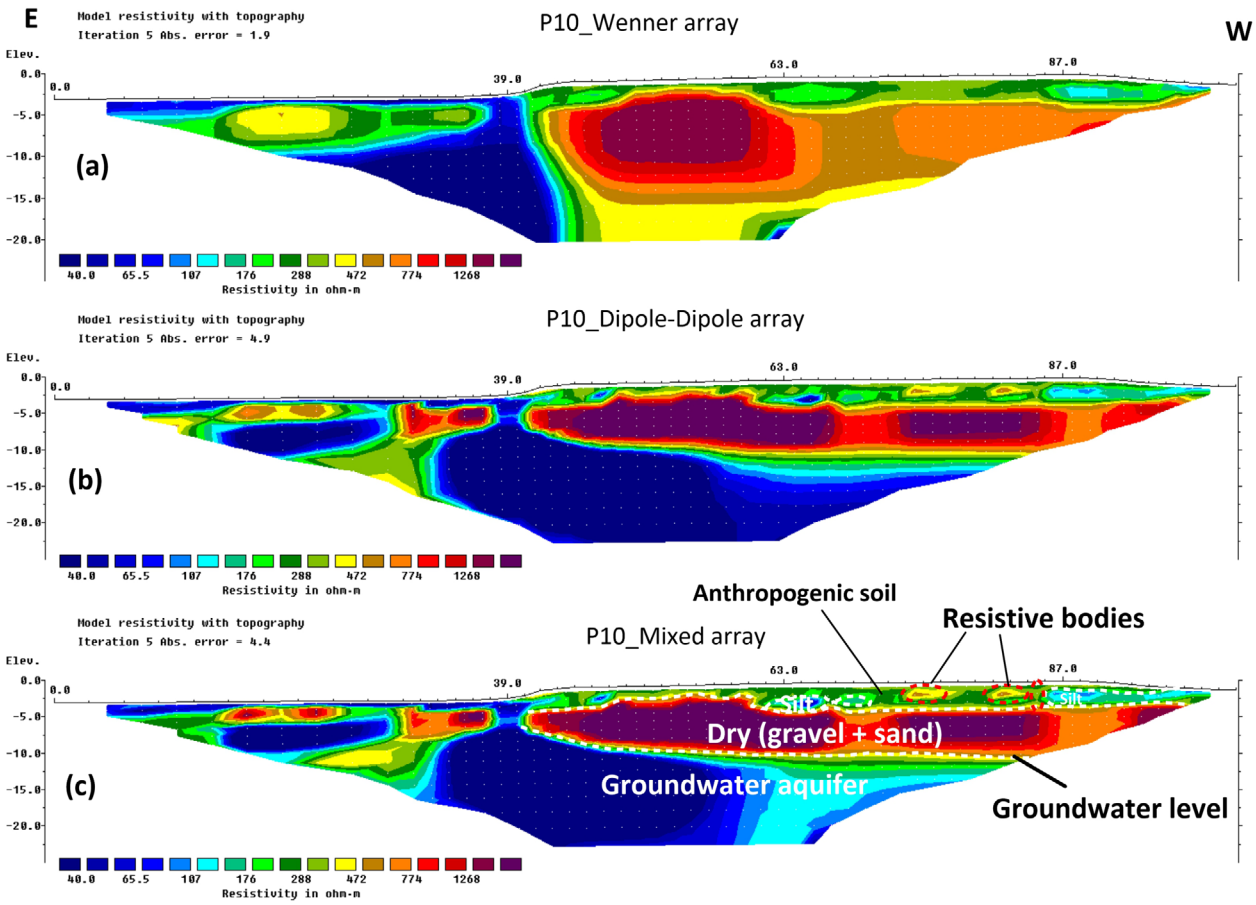

Figure 9 Inversion results of 2D ERT of profile P10 (Fig. 5) in the E–W direction using robust (blocky) inversion using (a) Wenner, (b) dipole–dipole and (c) non-conventional mixed arrays

high-resistivity layer (>700 Ωm up to several thousand Ωm) that can be associated with a dry gravel and sand formation. It reaches a depth of 8–10 m, coinciding with the groundwater table level in the area. (iv) A relatively low resistivity layer representing the base of the geoelectric section and the gravelly coarse sand groundwater aquifer in the area. This layer could be affected by salt contamination caused by salt stones situated at the location, where the topographic change is noticed on profile P10 (at a distance of 40.5 m from the beginning of the profile). Salt licks have been used by farmers for their cattle for a long time. Moreover, an accumulation of washed fertilizers and cow manure in this local depression could be an additional reason for the reduction of resistivity values. It is worth mentioning that small-scale archaeological remains cannot be seen clearly along this profile due to the relatively large electrode spacing of 1.5 m. By comparison, the resistive bodies of the first layer cannot be seen on the 2D resistivity model inverted from the Wenner array. Furthermore, the 2D inverted resistivity model from the mixed array somehow resembles the 2D inverted resistivity model obtained from the dipole–dipole array. Despite the long time required for data collection, the mixed array procedure significantly increases the resolution of subsurface images with respect to other configurations.

In most of the ERT profiles, a superficial layer was detected with a thickness of up to 2 m, characterized by an average resistivity value of 300 Ωm. Within this layer, local structures with resistivities exceeding 350 Ωm were detected and interpreted as anthropogenic/manmade. Figure 10 shows the inversion results after five iterations along profile P12 with an absolute error of 1.79. The sequence of the four geoelectric layers in addition to five resistive objects is clearly seen along this profile. These resistive bodies are in agreement with highly magnetic anomalies or with magnetic edges of the gradiometer

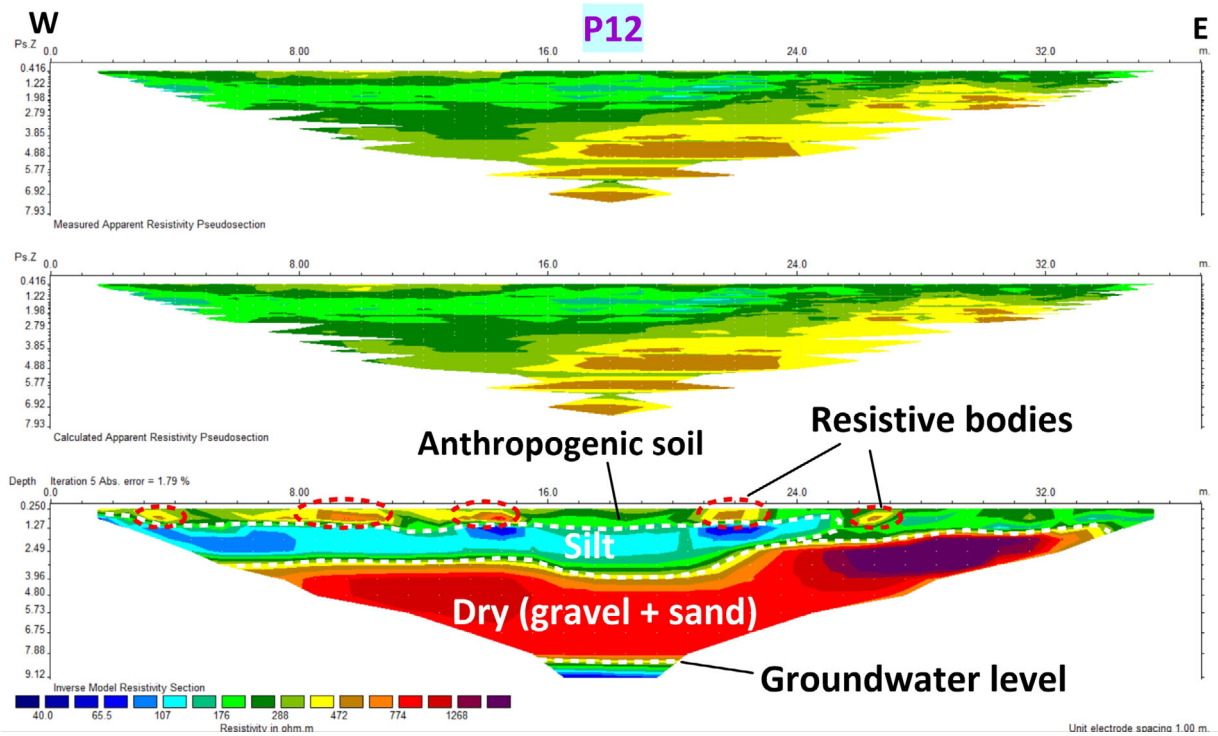

Figure 10 Measured and calculated apparent resistivity pseudosections of profile P12 using non-conventional mixed array and the result of robust inversion of the ERT data after five iterations (absolute error = 1.79)

image (Fig. 6b). Additionally, the groundwater level is detected at a depth of around 8.5 m. The 2D resistivity inverted models along profiles P1 to P9 are presented in Figures 11 and 12.

Combined interpretation of magnetic and electrical resistivity tomography data

Most of the resistive objects along profiles P1, P2, P3 and P9 (Fig. 11) are in agreement with the boundaries of the magnetic anomalies in Figure 6(b). For example, the resistive structures along profile P1 between distance 13 m and distance 25 m are coincident with the northern edge of the magnetic zone 1. ERT profile P8 (Fig. 12) has a resistive zone at a distance between 7.5 and 9.0 m from the beginning of the profile. This zone coincides with the highly magnetic anomaly B1 in Figures 6(b) and 8. A resistive structure consisting of two resistive bodies located on top of each other is imaged at a 12-m distance from the beginning of profile P6 (Fig. 12). It reaches a depth of up to 1.3 m from the ground surface. The same structure can be seen on profile P7 (Fig. 12) and also on profile P5, but as one resistive body. Two resistive bodies are detected along profile P4. The highly magnetic body B5 (Fig. 8) is confirmed by highly resistive anomalies along profiles P3 and P11. The inverted 2D ERT resistivity models from all profiles are combined into a 3D perspective (Fig. 13). Several high resistivity anomalies appear on this fence diagram. Some of them are probably related to possibly buried vestiges of walls and structures like tombs. The most interesting is the high resistivity anomalies corresponding with the negative magnetic belt between the two magnetic zones. They extend in a west–east direction and can be seen along profiles P6, P5, P7 and P4. These resistive structures could possibly be interpreted as the southern wall of the north building and/or the parallel northern wall of the southern one. Another interesting resistive structure trending south–north was detected along profiles P3, P12, P2 and P11 and can possibly be interpreted as an inner wall of the southern building. This resistive structure is also corresponding with a negative magnetic anomaly. Further, a part of the eastern wall of the southern building shows the same behavior with high resistive and negative magnetic anomalies. Several resistive features representing the southern wall can be seen on this fence diagram. Most of the high resistivity anomalies are reflecting subsurface features possibly having man-made archaeological structures such as resistive anomalies corresponding with high magnetic anomalies of B1, B5, B6 and B9. By contrast, some

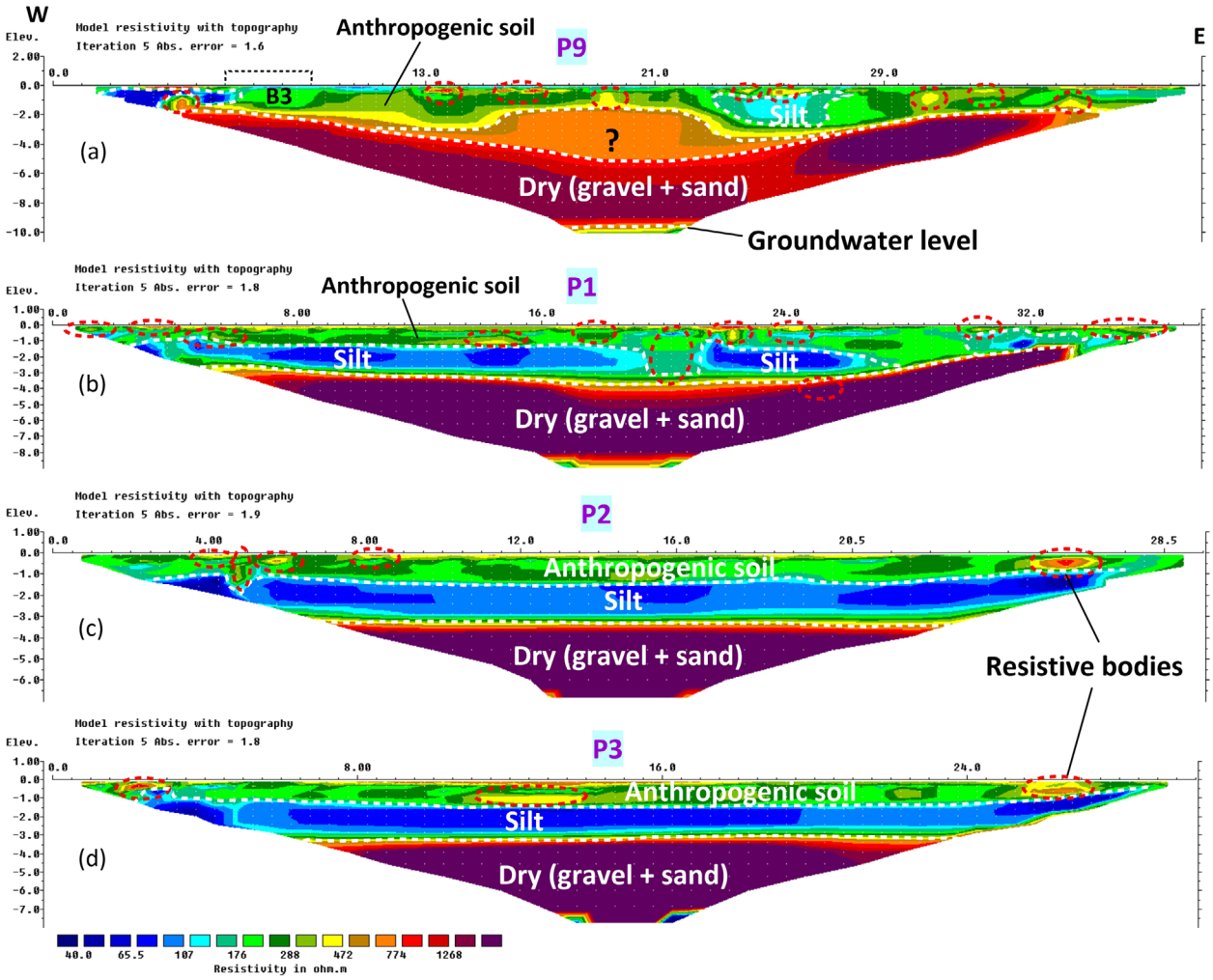

Figure 11 2D resistivity inverted models along profiles (a) P9, (b) P1, (c) P2 and (d) P3 using robust inversion

relatively conductive anomalies corresponding with high magnetic anomalies such as B3 and B7 might refer to ancient ruins. This can occur when the infill materials have a higher moisture content than the surroundings. In general, three classes of combined interpretation of ERT/magnetic anomalies can be identified: (i) resistive structures with high magnetic values such as B5 and B6; (ii) conductive structures with high magnetic values like anomalies B3 and B7; and (iii) resistive structures with slightly low/negative magnetic values such as the northern border (between zones 1 and 2) of the potential south building.

DISCUSSION

In this study, we performed a preliminary geophysical exploration on an archaeological site in Norf in order to delineate buried features using magnetic and ERT methods. The magnetic method can provide valuable information of subsurface remains found in a host medium with sufficient magnetic contrast. On the other hand, the geoelectric survey is concerned with the determination of the buried subsurface structures based on the presence of variations in resistivities. Despite the fact that each of the used methods provides independently useful geophysical information, the combination of the two methods and the joint interpretation of the observed anomalies can provide a more realistic perception of the subsurface structure and buried features (physical properties, dimensions, depths, etc.). The main objective of the geophysical survey was to verify the hypothesis of the presence of remains belong to an ancient church building and to determine its boundaries.

Generally, burned features can produce strong magnetic anomalies because of thermo-remanent magnetism

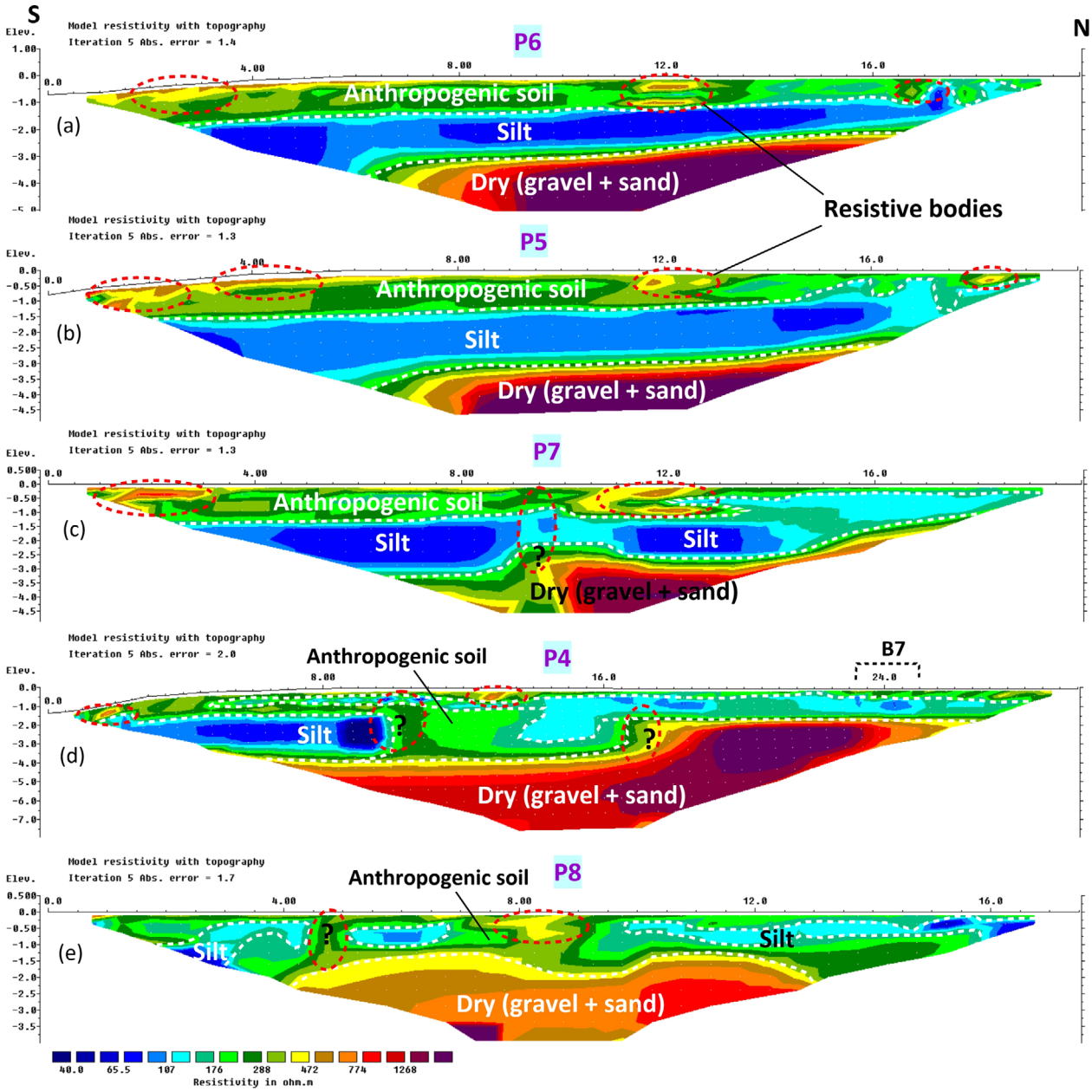

Figure 12 2D resistivity inverted models along profiles (a) P6, (b) P5, (c) P7, (d) P4 and (e) P8 using robust inversion

(Weymouth, 1986). Therefore, the destruction of the church by fire in 1585 possibly played a role in increasing the thermoremanent magnetization of materials and can be one of the interpretations of the high magnetic values in the surveyed area. Several causative bodies were imaged by both magnetic and ERT data at shallow depths down to 2 m. The observed anomalies characterized by high resistivity and low/negative magnetization values probably refer to walls, whereas strong positive mono-polar and dipolar magnetic anomalies corresponding with high resistivity values may indicate tomb-like structures and other magnetic sources. An exception can occur when the filling materials of tombs have resistivity values lower than the resistivity of the host medium. The RTP vertical gradient map (Fig. 6b) and the analytic signal map (Fig. 8) show nine magnetic anomalies (labelled B1–B9) having relatively higher magnetic intensity values than their surroundings and being clearly distinguishable from each other. The most prominent features in the RTP vertical gradient magnetic map

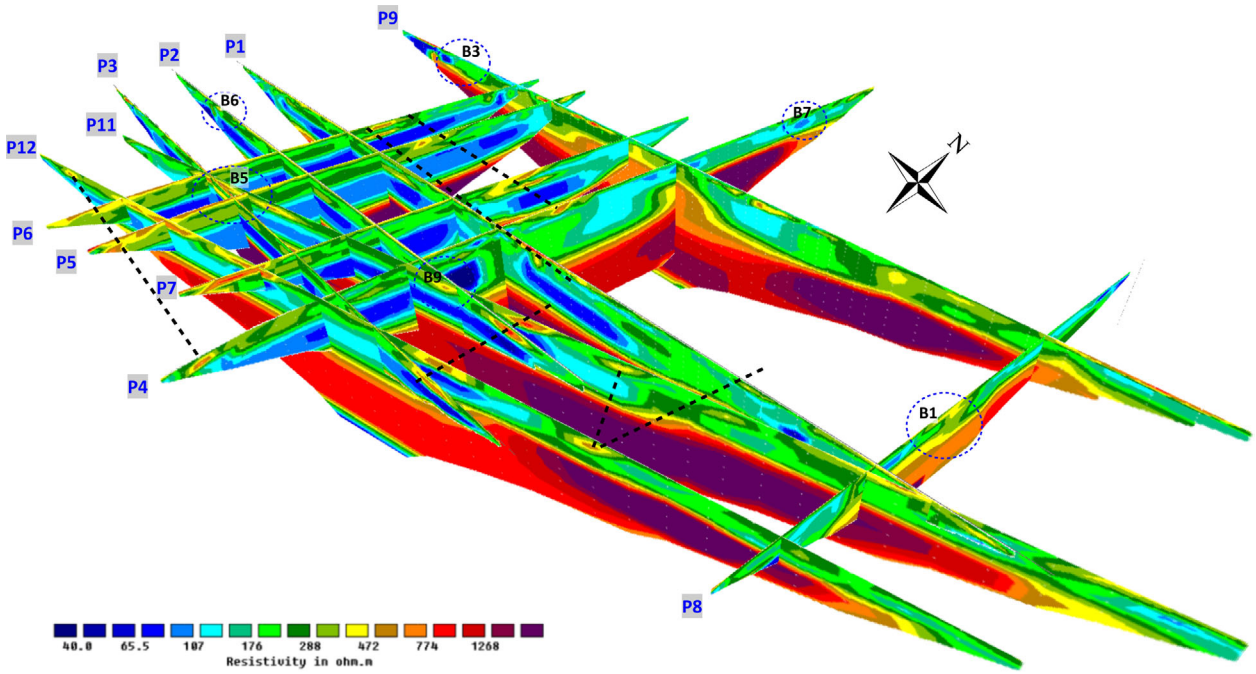

Figure 13 3D resistivity fence diagram of the archaeological site in Norf. Significant resistive structures are connected by dashed lines. Selected magnetic anomalies are also presented

(Fig. 6b) are a group of large anomalies of two magnetic polarities (B1–B4). Three of them (B1–B3) distribute on a line trending nearly in the E–W direction. They are represented by highly magnetic anomalies on the analytical signal map (Fig. 8). These dipolar magnetic anomalies can be interpreted as metallic objects within the subsurface. The dipolar nature of these magnetic anomalies may reflect a true plunging towards the north–northwest. However, we also expect a considerable influence of remanent magnetization on our magnetic data, but we can still argue that the RTP filter should create a less complex picture than the vertical gradient map owing to its effect on the induced component of magnetization in the survey area. Furthermore, the AS method effectively maps the locations of the edges of a shallow magnetic body irrespective of the orientation of the body's magnetization (Roest *et al.*, 1992). This makes the AS a powerful tool especially in places of unknown magnetization direction. Two distinct magnetic zones can be distinguished on the RTP vertical gradient magnetic map based on the sharp change of magnetic values from negative to positive anomalies. The boundaries between these magnetic zones are remarkably distinguished. The delineated features in the south zone (zone 1) of the vertical gradient magnetic map probably belong to the ancient church. The northern zone (zone 2) of the magnetic map, on the other hand, may be associated with another manmade structure parallel to the ancient church, possibly an older version of it. In the latter case, the destroyed by a fire can heat the materials enough to be re-magnetized and to produce magnetic anomalies with large amplitudes. Therefore, a high priority should be given to magnetic surveys if burned structures are explored (Bevan, 2006). Another possible explanation for zone 2 could be the paving of the yard near the church with bricks which produce irregular and rather complex magnetic anomalies because they are oriented in several directions different from those when they were made.

The depths of the magnetic causative sources were calculated by transferring the magnetic data to the frequency domain using FFT and then calculating the power spectrum. Calculations show that the depth of magnetic structures is about 0.85 m. The ERT method complements the magnetic measurements because it provides information about the deeper subsurface and is also sensitive to the change in resistivity in the subsurface. The results of the ERT survey show the presence of four geoelectric layers, which correspond well with the known geologic layers. The most important layer is the anthropogenic soil, which contains the target archaeological relics. Several resistive structures, which can be associated with man-made materials, were determined along the ERT profiles. We integrated geophysical information we obtained in a unique map and constructed a hypothetical archaeological subsurface scheme

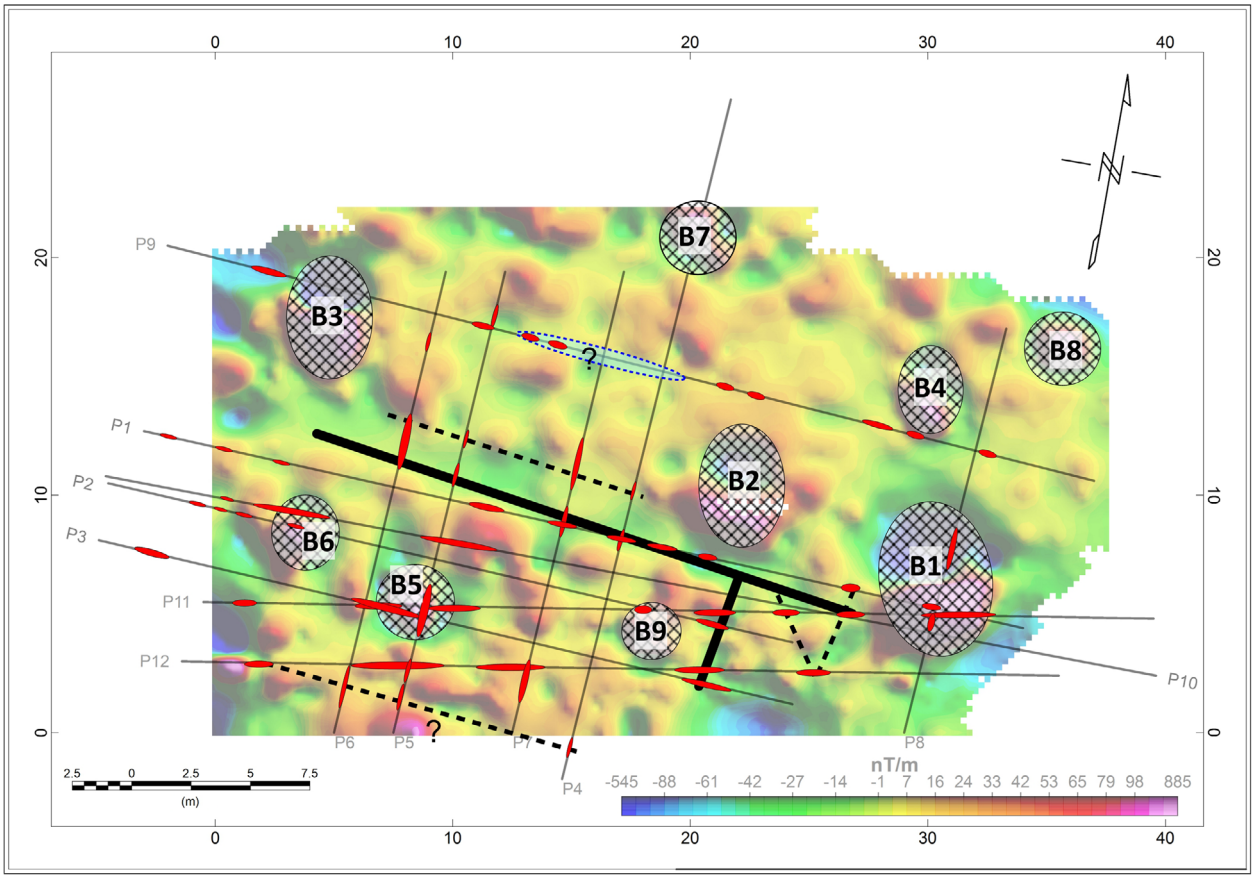

Figure 14 The hypothetical final map of the possible ancient buildings and features at the Norf archaeological site inferred from the magnetic and ERT results. The RTP magnetic map and ERT profiles are depicted in the background. Magnetic anomalies B1–B4 are interpreted as possible metallic bodies in the subsurface whereas magnetic anomalies marked by B5–B9 are associated with high-amplitude magnetic sources. The possible boundary walls of the potential building are marked on the map with thick black lines. Dashed black lines show the expected possible walls of lesser reliability. The red elongated spots mark the locations of the resistive anomalies

(Fig. 14). The locations of the interpreted walls of the potential buildings are drawn in dotted and solid black lines. However, the boundaries of the remains could not be identified completely using the magnetic data due to the accumulation and/or removal of magnetic structures over several centuries and also because the investigated site is located in an urban area where sources of noise can be expected. Only some parts of the features interpreted as walls were confirmed by both methods. Moreover, the magnetic field produced by the interpreted metallic bodies B1 and B2 probably conceals the magnetic anomalies produced by the walls as they are believed to be newer than the potential buildings. The most important feature of this sketch (Fig. 14) is the negative magnetic belt located between the two highly magnetic zones and corresponding to highly resistive structures which may reflect low or non-magnetic sandstone materials. Unfortunately, there exist no previous studies in the area to confirm this information. Moreover, isolated high positive mono-polar and dipolar magnetic anomalies in addition to high resistivity values can probably indicate tomb-like structures. Low resistivity values of graves may be expected in the case that the infill materials have lower resistivity values than the surrounding soil. This can be seen in the case of the highly magnetic body B7, where the ERT suggests a structure of low resistivity value at a depth of about 1 m that could be interpreted as a grave filled with loose and wet sediment. However, in some places of the site, there is no obvious correlation between ERT and magnetic anomalies. This hints at the strengths and weaknesses of the used archaeogeophysical techniques, especially the magnetic method in such an urban area. In this regard, it is worth noting that the magnetic survey has an important role in designing the ERT survey and also in detecting some borders of the

old church in zone 1 which is in coincidence with the results of the ERT survey. Hence, the archaeological interpretation in the present study was mainly based on those results supported by both techniques.

CONCLUSIONS

In conclusion, we have presented and discussed the results of a combined geophysical survey consisting of vertical magnetic gradient and ERT measurements carried out on an archaeological site in Neuss-Norf, Germany. The designing of the ERT measurements was based on the results of the magnetic survey. The geophysical survey shows that the causative sources of the anomalies in the investigated archaeological site are relatively shallow and reach depths of up to 2 m. Moreover, detailed subsurface geological information was inferred using geoelectric imaging, which is more or less in agreement with available information. A detailed archaeological map was constructed showing the potential locations of the ancient St. Andreas church and the assumed surrounding features. The combined inversion has produced better lateral and vertical resolution of the 2D subsurface resistivity image when compared to the inversion results obtained from dipole–dipole and Wenner array separately. Additionally, the present study highlights the importance of using exploration approaches based on a combination of different geophysical techniques, and the effectiveness of the joint interpretation of results to characterize subsurface structures in a more realistic way. The interpretation of the results of our geophysical investigation and the hypothesis of the presence of an ancient church as well as an earlier version can only be corroborated through subsequent archaeological excavations. Further geophysical studies, such as GPR survey and/or detailed 3D ERT measurements on selected anomalies, should provide more details about the buried archaeological relics.

ACKNOWLEDGEMENTS

The authors are thankful to the local homeland society Heimatverein Norf e.V. for facilitating the procedures in order to carry out this research, for their kind collaboration and making information from the historic archive of archdiocese Cologne available to us. We extend our thanks to S. Schiebel and L. Reineccius for their great contributions to the fieldwork. Special thanks go to Dr. C. Weber and Dr. K. Striewe for their comprehensive archaeological answers and constructive suggestions. We thank the Editor-in-Chief Dr. P. Tsourlos, Associate Editor Dr. N. Papadopoulos, and anonymous reviewers for their great suggestions and comments, which helped us to improve and clarify our manuscript. The field measurements were financed by the Institute of Geophysics and Meteorology, University of Cologne. The authors acknowledge the financial support by the Volkswagen Foundation.

Open access funding enabled and organized by Projekt DEAL.

CONFLICTS OF INTEREST

The authors declare that there is no conflict of interest.

DATA AVAILABILITY STATEMENT

The data that support the findings of this study are available from the corresponding author upon reasonable request.

ORCID


Ismael M. Ibraheem
https://orcid.org/0000-0001-6228-246X

REFERENCES

ABEM (2010) ABEM instruction manual, Terrameter SAS 4000 /SAS 1000, 2010-06-04, ABEM Printed Matter No. 93109. https://wwwguidelinegeoc.cdn.triggerfish.cloud/uploads/2016/03/Manual_Terrameter.pdf.

Akca, İ., Balkaya, Ç., Pülz, A., Alanyalı, H.S. and Kaya, M.A. (2019) Integrated geophysical investigations to reconstruct the archaeological features in the episcopal district of Side (Antalya, Southern Turkey). *Journal of Applied Geophysics*, 163, 22–30.

Arisoy, M. and Dikmen, Ü. (2013) Edge detection of magnetic sources using enhanced total horizontal derivative of the Tilt angle. *Bulletin of the Earth Sciences Application and Research Centre of Hacettepe University*, 34(1), 73–82.

Ayad, A. and Bakkali, S. (2018) Analysis of the magnetic anomalies of buried archaeological ovens of Aïn Kerouach (Morocco). *International Journal of Geophysics*, 2018, 9741950. https://doi.org/10.1155/2018/9741950.

Baranov, V. and Naudy, H. (1964) Numerical calculation of the formula for reduction to the magnetic pole . *Geophysics*, 22, 359–383.

Batayneh, A., Khataibeh, J., Alrshdan, H., Tobasi, U. and Al-Jahed, N. (2007) The use of microgravity, magnetometry and resistivity surveys for the characterization and preservation of an archaeological site at Umm er-Rasas. *Jordan. Archaeological Prospection*, 14(1), 60–70.

Berge, M.A. and Drahor, M.G. (2011) Electrical resistivity tomography investigations of multilayered archaeological settlements: part i – modelling. *Archaeological Prospection*, 18, 159–171.

Bevan, B.W. (2006) Geophysical exploration for buried buildings. *Historical Archaeology*, 40(4), 27–50. https://doi.org/10.1007/BF03376739.

Bhattacharyya, B.K. (1966) Continuous spectrum of total magnetic field anomaly due to a rectangular prismatic body. *Geophysics*, 31(1), 97–121.

Billings, S.D., Pasion, C., Walker, S. and Beran, L. (2006) Magnetic models of unexploded ordnance. *IEEE Transactions on Geoscience and Remote Sensing*, 44(8), 2115–2124. https://doi.org/10.1109/TGRS.2006.872905.

Boele, A. (1997) Die St. Lambertus Kapelle in Ramrath. Altehrwürdige Gebetsstätte und kunsthistorisches Kleinod. Beiträge zur Geschichte der Gemeinde Rommerskirchen, Bd. II. Dormagen: Verlag Rommerskirchen (in German).

Cardarelli, E., Fischanger, F. and Piro, S. (2008) Integrated geophysical survey to detect buried structures for archaeological prospecting. A case-history at Sabine Necropolis (Rome, Italy). *Near Surface Geophysics*, 6(26), 15–20.

Cassano, E. and Rocca, F. (1975) Interpretation of magnetic anomalies using spectral estimation techniques. *Geophysical Prospecting*, 23(4), 663–681.

Caminale, M. and Gallo, D. (2008) High-resolution magnetic survey in a quasi-urban environment. *Near Surface Geophysics*, 6(2), 97–103.

Claerbout, J.F. and Muir, F. (1973) Robust modeling with erratic data. *Geophysics*, 38, 826–844.

Cozzolino, M., Di Giovanni, E., Mauriello, P., Piro, S. and Zamuner, D. (2018) *Geophysical Methods for Cultural Heritage Management*. Cham, Switzerland: Springer International Publishing, 211 p.

Dahlin, T. and Zhou, B. (2004) A numerical comparison of 2D resistivity imaging with 10 electrode arrays. *Geophysical Prospecting*, 52, 379–398.

Di Maio, R., La Manna, M. and Piegari, E. (2016) 3D reconstruction of buried structures from magnetic, electromagnetic and ERT data: Example from the archaeological site of Phaistos (Crete, Greece). *Archaeological Prospection*, 23(1), 3–13.

Drahor, M.G. (2019) Integrated geophysical investigations in archaeological sites: case studies from Turkey. In: G. El-Qady and M. Metwaly ((Eds.) *Archaeogeophysics – State of the Art and Case Studies*. Cham, Switzerland: Springer International Publishing, pp. 27–68.

Drahor, M.G., Berge, M.A., Kurtulmuş, T.Ö., Hartmann, M. and Speidel, M.A. (2008) Magnetic and electrical resistivity tomography investigations in a Roman legionary camp site (Legio IV Scythica) in Zeugma, Southeastern Anatolia, Turkey. *Archaeological Prospection*, 15(3), 159–186.

El Emam, A., Abdallatif, T., Suh, M. and Odah, H. (2014) Delineation of Egyptian mud bricks using magnetic gradiometer techniques. *Arabian Journal of Geosciences*, 7, 489–503.

El-Qady, G., Metwaly, M. and Drahor, M.G. (2019) Geophysical techniques applied in archaeology. In: G. El-Qady and M. Metwaly ((Eds.) *Archaeogeophysics – State of the Art and Case Studies*. Springer International Publishing, 1–25.

Emsbach, K. and Tauch, M. (1986) Kirchen, Klöster und Kapellen im Kreis Neuss., Köln: Rheinland-Verlag, 192 (in German)

Epov, M.I., Molodin, V.I., Manshtein, A.K., Balkov, E.V., Dyad'kov, P.G., Matasova, G.G., et al. (2016) Integrated archeological and geophysical studies in West Siberia. *Russian Geology and Geophysics*, 57(3), 473–482.

Fauchard, C., Saley, A.D., Camerlynck, C., Fargier, Y., Antoine, R. and Thérain, P.-F. (2018) Discovery of the Romanesque church of the Abbey of our lady of Bec (Le Bec-Hellouin, Normandy, France) by means of geophysical methods. *Archaeological Prospection*, 25(4), 315–328.

Fedi, M., Quarta, T. and De Santis, A. (1997) Inherent power–law behavior of magnetic field power spectra from Spector and Grant ensemble. *Geophysics*, 62(4), 1143–1150.

Fischer, J. (1989) *Unser Norf, Stadtsparkasse Neuss*. Neusser Druckerei und Verlag, Neuss, Germany: Neusser Druckerei und Verlag (in German).

Florio, G., Cella, F., Speranza, L., Castaldo, R., Benoit, R.P. and Palermo, R. (2019) Multiscale techniques for 3D imaging of magnetic data for archaeo-geophysical investigations in the Middle East: The case of Tell Barri (Syria). *Archaeological Prospection*, 26(4), 379–395.

Geologischer Dienst NRW (1931) Geologische Karte von Preußen und benachbarten deutschen Ländern, Blatt 4806 Neuss. Accessed 12 February 2020. Data licence Germany– attribution –Version 2.0 (in German).

Geologischer Dienst NRW (1983) Hydrogeologische Karte von Nordrhein-Westfahlen, Blatt 4806 Neuss. Accessed 12 February 2020. Data licence Germany – attribution – Version 2.0 (in German).

Getaneh, A., Haile, T. and Sernicola, L. (2018) Three-dimensional modelling of a pre-Aksumite settlement at the archaeological site of Seglamen, Aksum, northern Ethiopia using integrated geophysical techniques. *Archaeological Prospection*, 25(3), 231–241.

Ghazala, H.H., Ibraheem, I.M., Haggag, M. and Lamees, M. (2018) An integrated approach to evaluate the development possibility around Sohag governorate, Egypt using potential field data. *Arabian Journal of Geosciences*, 11, 194. https://doi.org/10.1007/s12517-018-3535-1.

Gündoğdu, N.Y., Candansayar, M.E. and Genç, E. (2017) Rescue archaeology application: Investigation of Kuriki mound archaeological area (Batman, SE Turkey) by using direct current resistivity and magnetic methods. *Journal of Environmental and Engineering Geophysics*, 22(2), 177–189.

Hahn, A., Kind, E.G. and Mishra, D.C. (1976) Depth estimation of magnetic sources by means of Fourier amplitude spectra. *Geophysical Prospecting*, 24(2), 287–306.

Hawamdeh, A., Jaradat, R. and Alsaad, Z. (2015) Integrated application of geophysical methods for investigation of the Al-Berktain archaeological site in the city of Jerash. *Jordan. Environmental Earth Sciences*, 73(7), 3665–3674.

Hegyi, A., Vernica, M.-M. and Drăguţ, L. (2019) An object-based approach to support the automatic delineation of magnetic anomalies. *Archaeological Prospection*, 27(1), 3–12. https://doi.org/10.1002/arp.1752.

Hinze, W.J., Von Frese, R.R.B. and Saad, A.H. (2013) *Gravity and Magnetic Exploration: Principles, Practices, and Applications*. Cambridge University Press.

Ibraheem, I.M., Haggag, M. and Tezkan, B. (2019a) Edge detectors as structural imaging tools using aeromagnetic data: A case study of Sohag area, Egypt. *Geosciences*, 9(5), 211.

Ibraheem, I., Tezkan, B. and Bergers, R. (2019b) Imaging of a waste deposit site near Cologne city, Germany using magnetic and ERT methods. 25th European Meeting of Environmental and Engineering Geophysics, Near Surface Geoscience Conference & Exhibition, The Hague, The Netherlands. https://doi.org/10.3997/2214-4609.201902492.

Ibraheem, I.M., Gurk, M., Tougiannidis, N. and Tezkan, B. (2018a) Subsurface imaging of the Neogene Mygdonian basin, Greece using magnetic data. *Journal of Pure and Applied Geophysics*, 175(8), 2955–2973.

Ibraheem, I.M., Elawadi, E.A. and El-Qady, G.M. (2018b) Structural interpretation of aeromagnetic data for the Wadi El Natrun area, Northwestern Desert, Egypt. *Journal of African Earth Sciences*, 139, 14–25.

Ibraheem, I.M., Tezkan, B. and Bergers, R. (2021) Integrated Interpretation of magnetic and ERT data to characterize a landfill in the north-west of Cologne, Germany. *Pure and Applied Geophysics*, https://doi.org/10.1007/s00024-021-02750-x

Isles, D.J. and Rankin, L.R. (2013) *Geological Interpretation of Aeromagnetic Data*. Canberra, Australia: CSIRO, 365 p.

Jeng, Y., Lee, Y.L., Chen, C.Y. and Lin, M.J. (2003) Integrated signal enhancements in magnetic investigation in archaeology. *Journal of Applied Geophysics*, 53, 31–48.

Karaaslan, H. and Karavul, C. (2018) Usefulness of electrical and magnetic methods in finding buried structure of the Alabanda Ancient Cistern in Çine Town, Aydın City, Turkey. *Arabian Journal of Geosciences*, 11, 178.

Kaufmann, O. and Quinif, Y. (2001) An application of cone penetration tests and combined array 2D electrical resistivity to delineate cover-collapse sinkhole prone areas. In: B.F. Beck and J.G. Herring (Eds) *Geotechnical and Environmental Applications of Karst Geology and Hydrology*. Rotterdam, the Netherlands: Balkema, pp. 359–364.

Kivior, I. and Boyd, D. (1998) Interpretation of the aeromagnetic experimental survey in the Eromanga/Cooper basin. *Canadian Journal of Exploration Geophysics*, 34, 58–66.

Křivánek, R. (2019) The contribution of new geophysical measurements at the previously excavated Neolithic rondel area near Bylany, central Bohemia. *Archaeological Prospection*, 27, 39–52. https://doi.org/10.1002/arp.1755.

Lacomblet, T.J. (1840) Urkundenbuch für die Geschichte des Niederrheins oder des Erzstifts Cöln, der Fürstentümer Jülich und Berg, Geldern, Meurs, Cleve und Mark, und der Reichsstifte Elten, Essen und Werden. Aus den Quellen in dem Königlichen Provinzial-Archiv zu Düsseldorf und in den Kirchen- und Stadtarchiven der Provinz. Erster Band, Von dem Jahr 779 bis 1200 einschliesslich, Reprinted 1966, **1**, Aalen, 18. Düsseldorf : Wolf (in German).

Landesarchiv, N.R.W. (2020) Abtlg. Rheinland, Reichskammergericht AA 0627, Teil VI, Aktenzeichen: N 410/1119. Accessed at https://www.archive.nrw.de [accessed 25 February 2020] (in German).

Linsser, H. (1970) Remarks on the use of the magnetic gradiometer in oil exploration. *Geophysical Prospecting*, 18(1), 119–133.

Loke, M.H. (1999) *Electrical imaging surveys for environmental and engineering studies: a practical guide to 2-D and 3-D surveys*. Penang, Malaysia.

Loke, M.H. (2000) *Tutorial: 2-D and 3-D electrical imaging surveys*. Penang, Malaysia: Geotomo Software, Penang, 129 p.

Loke, M.H., (2020) *Tutorial: 2-D and 3-D electrical imaging surveys*. Penang, Malaysia: Geotomosoft Solutions, Malaysia. Available at: www.geotomosoft.com. Accessed 18 March 2020.

Loke, M.H., Acworth, I. and Dahlin, T. (2003) A comparison of smooth and blocky inversion methods in 2D electrical imaging surveys. *Exploration Geophysics*, 34, 182–187.

Lowrie, M. (2007) *Fundamentals of Geophysics*. New York: Cambridge University Press, 381 p.

Lulewicz, J., Thompson, V.D. and DePratter, C.B. (2019) Mapping Spanish settlement at Santa Elena, 1566–1587: an integrated archaeogeophysical approach. *Archaeological Prospection*, 26(3), 239–250.

Martinez, J., Rey, J., Gutiérrez, L.M., Novo, A., Ortiz, A.J., Alejo, M. and Galdón, J.M. (2015) Electrical resistivity imaging (ERI) and ground-penetrating radar (GPR) survey at the Giribaile site (upper Guadalquivir valley. southern Spain. *Journal of Applied Geophysics*, 123, 31–48.

Marzinkowski, H. (2020) Museum zeigt restaurierte Grabbeigaben, 11.02.2020. Available at: https://rp-online.de/nrw/staedte/neuss/clemens-sels-museum-in-neuss-zeigt-restaurierte-grabbeigaben-aus-dem-7-jahrhundert_aid-48740277. (in German). Accessed 19 February 2020.

Metzdorf, J. (2019) Die Straßen von Neuss, Lexikon zur Geschichte der Neusser Stadtteile, der Straßen, Wege, Plätze und ihrer Namen. Neuss: Schriftenreihe des Stadtarchivs Neuss, Bd. 22, Stadt Neuss Stadtarchiv, 854 Seiten (in German).

Milsom, J. and Eriksen, A. (2011) *Field Geophysics*, 4th edition. Chichester, UK: Wiley-Blackwell, 304 p.

Müller, C., Woelz, S., Ersoy, Y., Boyce, J., Jokisch, T., Wendt, G. and Rabbel, W. (2009) Ultra-high-resolution marine 2D–3D seismic investigation of the Liman Tepe/Karantina Island archaeological site (Urla/Turkey). *Journal of Applied Geophysics*, 68(1), 124–134.

Nabighian, M.N. (1972) The analytic signal of two-dimensional magnetic bodies with polygonal cross-section: Its properties and use for automated anomaly interpretation. *Geophysics*, 37(3), 507–517.

Orlando, L., Michetti, L.M., Marchesini, B.B., Papeschi, P. and Giannino, F. (2019) Dense georadar survey for a large-scale reconstruction of the archaeological site of Pyrgi (Santa Severa, Rome). *Archaeological Prospection*, 26(4), 369–377.

Oswin, J. (2009) *A Field Guide to Geophysics in Archaeology*. Chichester, UK: Springer-Praxis, 221 p.

Piro, S. (2009) Introduction to geophysics for archaeology. In: S. Campana and S. Piro ((Eds.) *Seeing the Unseen – Geophysics and Landscape Archaeology*. London: Taylor and Francis Group, 27–64.

Piro, S., Papale, E., Zamuner, D. and Kucukdemirci, M. (2019) Multimethodological approach to investigate urban and suburban archaeological sites. In R. Persico, S. Piro and N. Linford. *Innovation in Near-Surface Geophysics – Instrumentation, Application, and Data Processing Methods*. Elsevier, pp. 461–504.

Pütz, B. (1974) Nor apa, Norpe, Norf – Ein Dorf wächst in Jahrtausenden. Aufsätze und Berichte zur Geschichte einer rheinischen Wohn- und Industriegemeinde. Stadt Neuss, 336 S (in German).

Quesnel, Y., Jrad, A., Mocci, F., Gattacceca, J., Mathé, P.-E., Parisot, J.-C., et al. (2011) Geophysical signatures of a Roman and early medieval Necropolis. *Archaeological Prospection*, 18(2), 105–115.

Rabbel, W., Erkul, E., Stümpel, H., Wunderlich, T., Pašteka, R., Papco, J., et al. (2014) Discovery of a Byzantine Church in Iznik/Nicaea, Turkey: an educational case history of geophysical prospecting with combined methods in urban areas. *Archaeological Prospection*, 22(1), 1–20.

Rajagopalan, S. (2003) Analytic signal vs. reduction to pole: solutions for low magnetic latitudes. *Exploration Geophysics*, 34(4), 257–262.

Remmen, K. (2013) Hieronymus Isenberg: Pfarrer in St. Peter Rosellen bei Neuss 1626–1639 /Instructiones de omnibus Ecclesiae Rosellanae iuribus A° Dni 1640 absolutae [transliteration of handwriting], Libelli Rhenani **46**, Köln: Erzbischöfl. Diözesan- und Dombibliothek, pp. 29–81 (in German).

Reynolds, J.M. (2011) *An Introduction to Applied and Environmental Geophysics*. 2nd edition, Wiley-Blackwell, Chichester, UK: Wiley-Blackwell, 712 p.

Rizzo, E., Chianese, D. and Lapenna, V. (2005) Magnetic, GPR and geoelectrical measurements for studying the archaeological site of 'Masseria Nigro' (Viggiano, southern Italy). *Near Surface Geophysics*, 3(1), 13–19.

Roest, W.R., Verhoef, J. and Pilkington, M. (1992) Magnetic interpretation using the 3-D analytic signal. *Geophysics*, 57(1), 116–125.

Sapia, V., Florindo, F., Marchetti, M. and Di Nezza, M. (2017) Fast geophysical prospection to map the archaeological site of Cocciano: Preliminary results. *Annals of Geophysics*, 60, Fast Track 6. https://doi.org/10.4401/ag-7406.

Sanchez, V., Li, Y., Nabighian, M. and Wright, D. (2006) Relative importance of magnetic moments in UXO clearance applications. SEG Annual Meeting, New Orleans, Louisiana, pp. 1381–1385. https://doi.org/10.1190/1.2369777.

Schmidt, A. (2009) Electrical and magnetic methods in archaeological prospection. In: S. Campana and S. Piro ((Eds.) *Seeing the Unseen – Geophysics and Landscape Archaeology*. Taylor and Francis Group, London: Taylor and Francis Group, pp. 67–81.

Scollar, I., Tabbagh, A., Hesse, A. and Herzog, I. (1990) *Archaeological Prospecting and Remote Sensing, Topics in Remote Sensing 2*. Cambridge: Cambridge University Press, pp. 375–516.

Sharma, P.V. (1997) *Environmental and Engineering Geophysics*. Cambridge: Cambridge University Press, pp. 78–79.

Siegmund, S. (1998) Merowingerzeit am Niederrhein, Die frühmittelalterlichen Funde aus dem Regierungsbezierk Düsseldorf und dem Kreis Heinsberg, Band 34. Rheinische Ausgrabungen, Köln: Rheinland-Verlag, pp. 335–336 (in German).

Spector, A. and Grant, F.S. (1970) Statistical models for interpretation of aeromagnetic data. *Geophysics*, 35, 293–302.

Telford, W.M., Geldart, L.P., Sheriff, R.E. and Keys, D.A. (1990) *Applied Geophysics*, 2nd edition. Cambridge, Cambridge University Press, 770 p.

Tsokas, G.N., Tsourlos, P.I., Kim, J.-H., Yi, M.-J., Vargemezis, G., Lefantzis, M., et al. (2018) ERT imaging of the interior of the huge tumulus of Kastas in Amphipolis (northern Greece). *Archaeological Prospection*, 25(4), 347–361.

Weber, C. (2020) LVR-Amt für Bodendenkmalpflege im Rheinland. Information about the archaeological background of the area was obtained through personal communications.

Weymouth, J.W. (1986) Archaeological site surveying program at the University of Nebraska. *Geophysics*, 51(3), 538–552

Wolke, R. and Schwetlick, H. (1988) Iteratively reweighted least-squares algorithms, convergence analysis, and numerical comparisons. *SIAM Journal of Scientific and Statistical Computations*, 9, 907–921.

Yilmaz, S., Balkaya, Ç., Çakmak, O. and Oksum, E. (2019) GPR and ERT explorations at the archaeological site of Kılıç village (Isparta, SW Turkey). *Journal of Applied Geophysics*, https://doi.org/10.1016/j.jappgeo.2019.103859.

Zhao, W., Forte, E., Pipan, M. and Tian, G. (2013) Ground penetrating radar (GPR) attribute analysis for archaeological prospection. *Journal of Applied Geophysics*, 97, 107–117.

Zhou, B. and Dahlin, T. (2003) Properties and effects of measurement errors on 2D resistivity imaging surveying. *Near Surface Geophysics*, 1, 105–117.

Zhou, W., Beck, B.F. and Adams, A.L. (2002) Effective electrode array in mapping karst hazards in electrical resistivity tomography. *Environmental Geology*, 42, 922–928. https://doi.org/10.1007/s00254-002-0594-z.

